FINAL TECHNICAL REPORT

PRECISION POINTING CONTROL SYSTEM

13900-6013-RU-00

1 JULY 1972

PPCS STAR TRACKER TEST

Contract No. NAS5-21111

Prepared for

NATIONAL AERONAUTICS AND SPACE ADMINISTRATION
GODDARD SPACE FLIGHT CENTER
Greenbelt, Maryland 20771

TRW
SYSTEMS GROUP

ONE SPACE PARK • REDONDO BEACH, CALIFORNIA 90278

FINAL TECHNICAL REPORT

PRECISION POINTING CONTROL SYSTEM

13900-6013-RU-00 1 JULY 1972

PPCS STAR TRACKER TEST

Contract No. NAS5-21111

Prepared for

NATIONAL AERONAUTICS AND SPACE ADMINISTRATION
GODDARD SPACE FLIGHT CENTER
Greenbelt, Maryland 20771

TRW
SYSTEMS GROUP

ONE SPACE PARK • REDONDO BEACH, CALIFORNIA 90278

TABLE OF CONTENTS

1.0 INTRODUCTION

This report describes the tests performed on the TRW precision star tracker. The unit tested was a two-axis gimballed star tracker designed to provide star LOS data to an accuracy of 1-2 sec. The tracker features a unique bearing system and utilizes thermal and mechanical symmetry techniques to achieve high precision which can be demonstrated in a one g environment. The test program included a laboratory evaluation of tracker functional operation, sensitivity, repeatibility, and thermal stability.

2.0 TEST DESCRIPTION

2.1 Test Objectives

The following test objectives were the goal of the test program:

- Perform measurements to verify certain design parameters of the tracker and compare to analytical results. (Sensor gain, FOV, Noise, Motor Torque, Bearing Friction, Inertias, Structural Frequencies)
- Demonstrate and evaluate tracker functional performance in all its operating modes (Slew, lock-on, track)
- Evaluate tracker repeatibility.
- Evaluate tracker long-term stability and thermal stability.

2.2 Test Specimen

The test specimen was a two-axis gimballed star tracker with a design goal of 1.3 $\widehat{\text{sec}}$ null stability and 0.35 $\widehat{\text{sec}}$ noise. The star tracker (Figure 1) consists of a two-axis gimballed drive and a null-seeking star sensor. Two control modes are used:

- Slew. The gimbals operate under computer control to point the star sensor in the vicinity of the star. Closed loop position control is obtained using Inductosyn gimbal angle readout.
- Track. The gimbals are controlled by star sensor error signals to point the star sensor at the star (null seeking). The gimbal angle readout is combined with the star sensor signals to obtain a measure of star LOS relative to the gimbal base.

The gimbal consists of four nearly identical drive housings connected via a structural I-beam ring. Each gimbal drive housing contains a single-ball bearing, a bearing suspension, a torque motor, two Inductosyn angle encoder plates and a

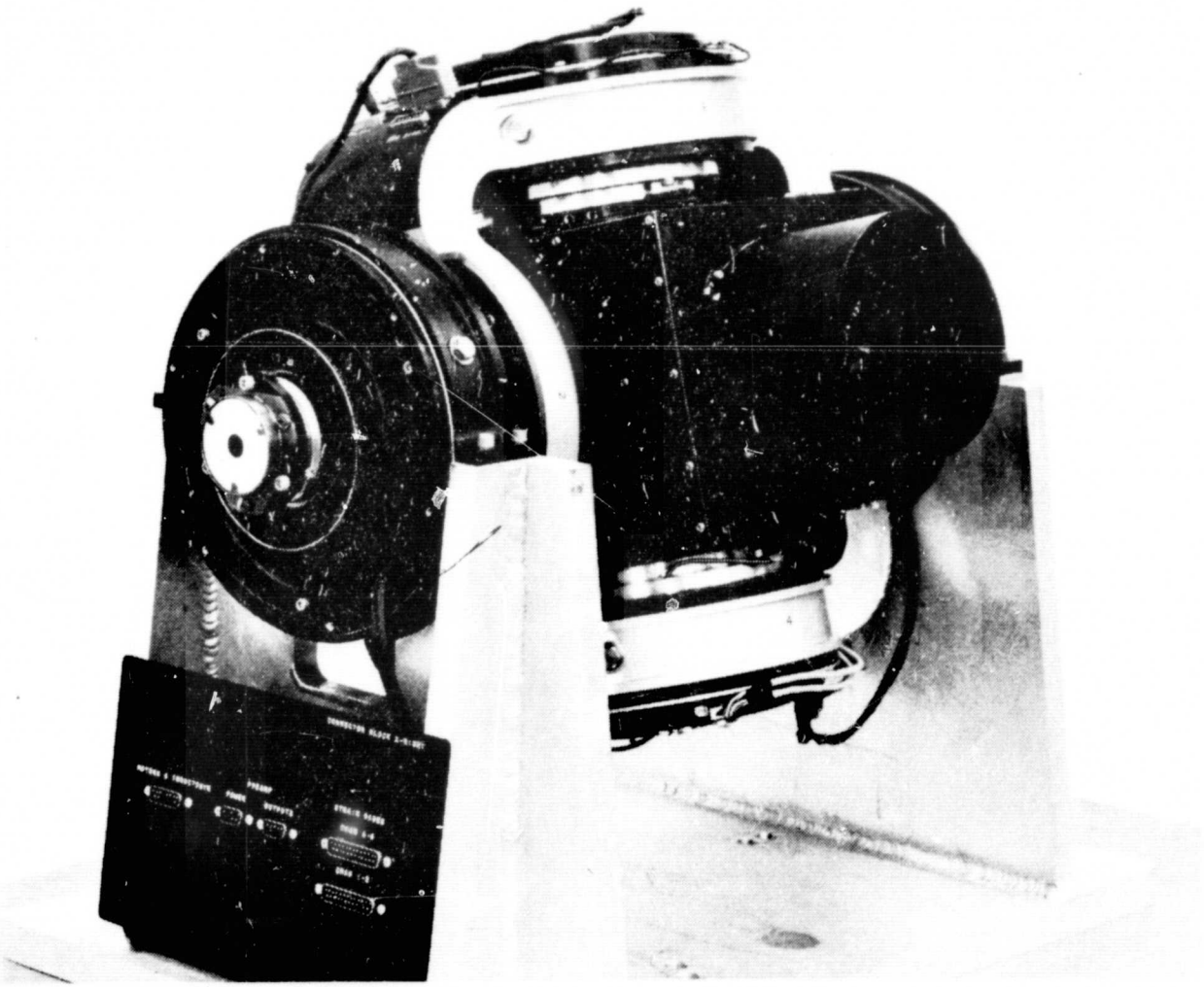

FIGURE 2-1. PPCS Star Tracker (Engineering Model)

FIGURE 1. PPCS STAR TRACKER

data link. Preamplifiers are packaged in the gimbal housings to amplify the low-level Inductosyn output signals.

The star sensor consists of an aluminum housing and sun shade with aluminum reflective optics, a photomultiplier detector, and integral electronics. Pertinent design and performance characteristics of the star tracker are summarized below:

Tracker Design Characteristics

Detector	F 4004 PMT (S20 cathode)
Sensor FOV	
Acquisition Mode	10 $\widehat{min}$ x 10 $\widehat{min}$
Track Mode	28 $\widehat{sec}$
Gimbal Freedom	$\pm$15 (IGA), $\pm$45° (OGA)
Optics	Folded Gregorian
Focal Length	2.54 meters
Aperture	54 cm^2
Tracking Bandwidth	25 Hz
Sensitivity	+3.5M A0 Star
Nearest Sun Angle	45°
Error Voltage Outputs	
Scale Factor	20 mv/arc sec
Linear Range	$\pm$5 $\widehat{min}$
Linearity	$\pm$5%
Gimbal Friction (Nominal)	15 in-oz (IGA), 30 in-oz (OGA)
Motor Torque (per Motor)	60 in-oz @ 18 v
Power	18 watts
Size	22 x 17 x 17 inches
Weight	56 pounds (aluminum)

Tracker Performance Characteristics

Accuracy (Track Mode)	
Sensor Electronic Bias	0.2 $\widehat{sec}$ (1σ)
Sensor Thermomechanical Bias	0.4 $\widehat{sec}$ (1σ)
Noise (+3.5 M star)	0.35 $\widehat{sec}$ (1σ)
Gimbal Bias Stability	1.0 $\widehat{sec}$
Encoder Repeatibility	0.63 $\widehat{sec}$
Gimbal Rates	
Slew	<4 deg/sec
Track	<0.2 deg/sec

During launch and initial carrier spacecraft orientation, the STA is caged. This is accomplished by driving the two gimbals to the extreme rotational angle (+50° outer and +20° inner), which brings axial stops to within 0.002" of contact and radial stops into actual contact. A mechanical detent holds the gimbal in this position until initial on-orbit use.

Initial star acquisition is accomplished by applying power to the STA and commanding suitable motor torques (computer commands to the Sensor Electronics Assembly, which appear as properly commutated motor analog voltages at the gimbal) to drive the gimbal so that the star sensor bore-sight is near ($\pm$3°, two axis) a desired star. Inductosyn gimbal angle readouts are compared to commanded gimbal angles (in the computer) for this operation. The gimbals are then driven in a programmed search pattern covering the $\pm$3° uncertainty region while the star sensor scans its acquisition field of view ($\pm$10 arc minutes) with a raster scan (0.25 sec/scan). The gimbal search rate is such that the star sensor scans each area twice. The second scan seeing a star brighter than a fixed lower threshold switches operation automatically to track mode (sensing and mode switch done in the star sensor electronics). In this mode, the sensor scan is reduced to a $\pm$28 arc sec cruciform pattern.

Upon entering track mode, the star sensor provides error signals relating its boresight to the star LOS. These error signals are used in the Sensor Electronics Assembly to drive the gimbals so as to null the boresight errors. This operating condition is maintained until the computer has obtained a star LOS reading (gimbal angles combined with star sensor error signals). Then a new star is sought by a similar process (with smaller uncertainty). After 5-10 such sightings, the computed attitude will converge to its pre-calibration value and acquisition will be completed.

A phase of calibration followed by normal mode operation will follow.

2.3 Test Facility

Two physical equipment layouts were used; one, a fixed base facility shown in Figure 2 for the repeatibility tests, and the other (Figure 3) for rate table tracking tests. Figures 4 and 5 are photographs of the test facility with star tracker in place.

Fixed Base

A layout of the facility is shown in Figure 2. A large (4' x 8' x 1') granite slab was used to support the STA and two 12-inch diameter, 500 inch focal length star stimulus. Optical reflecting surfaces were fixed to the outer gimbal and to

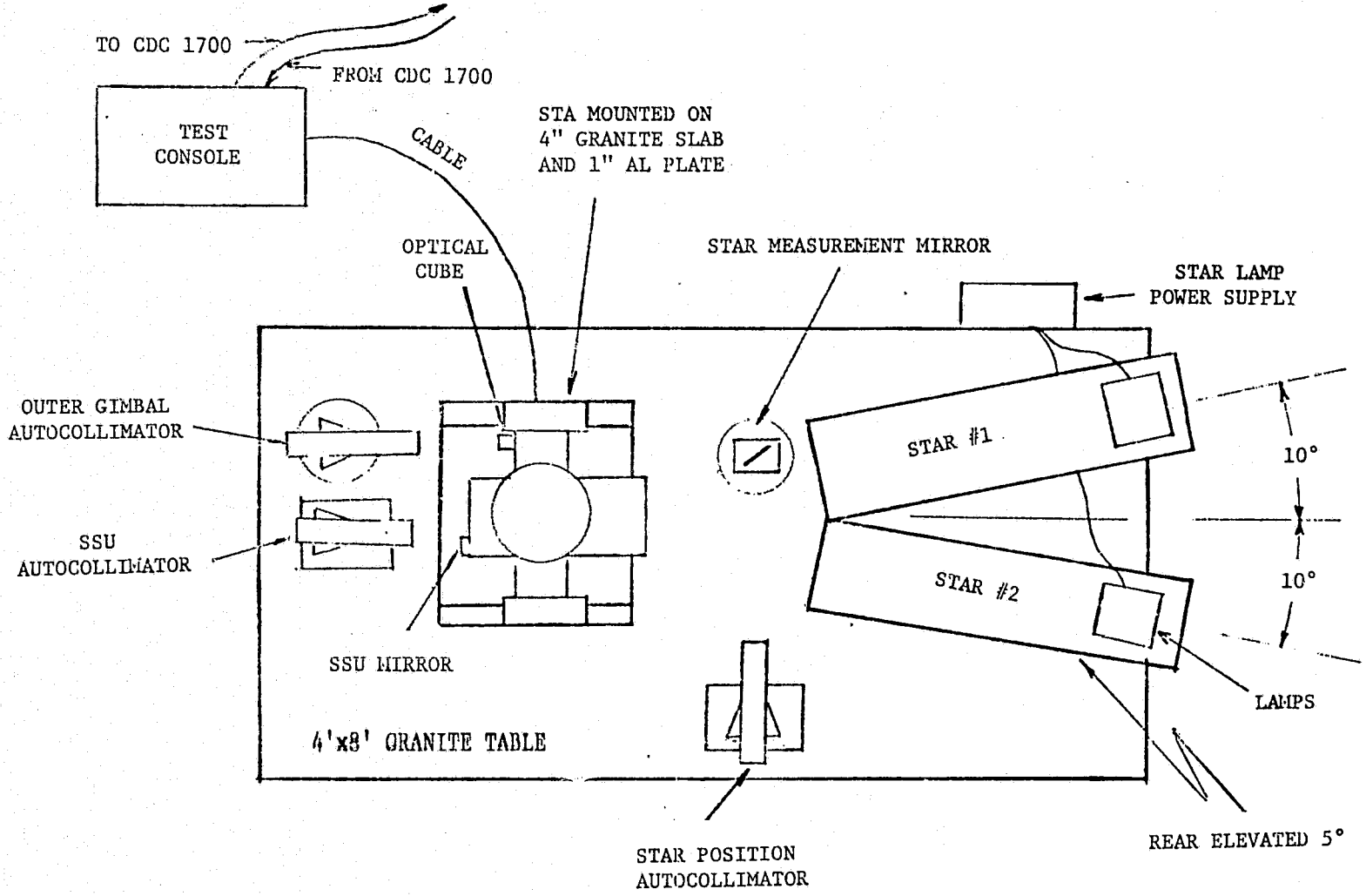

FIGURE 2. FIXED BASE TEST FACILITY

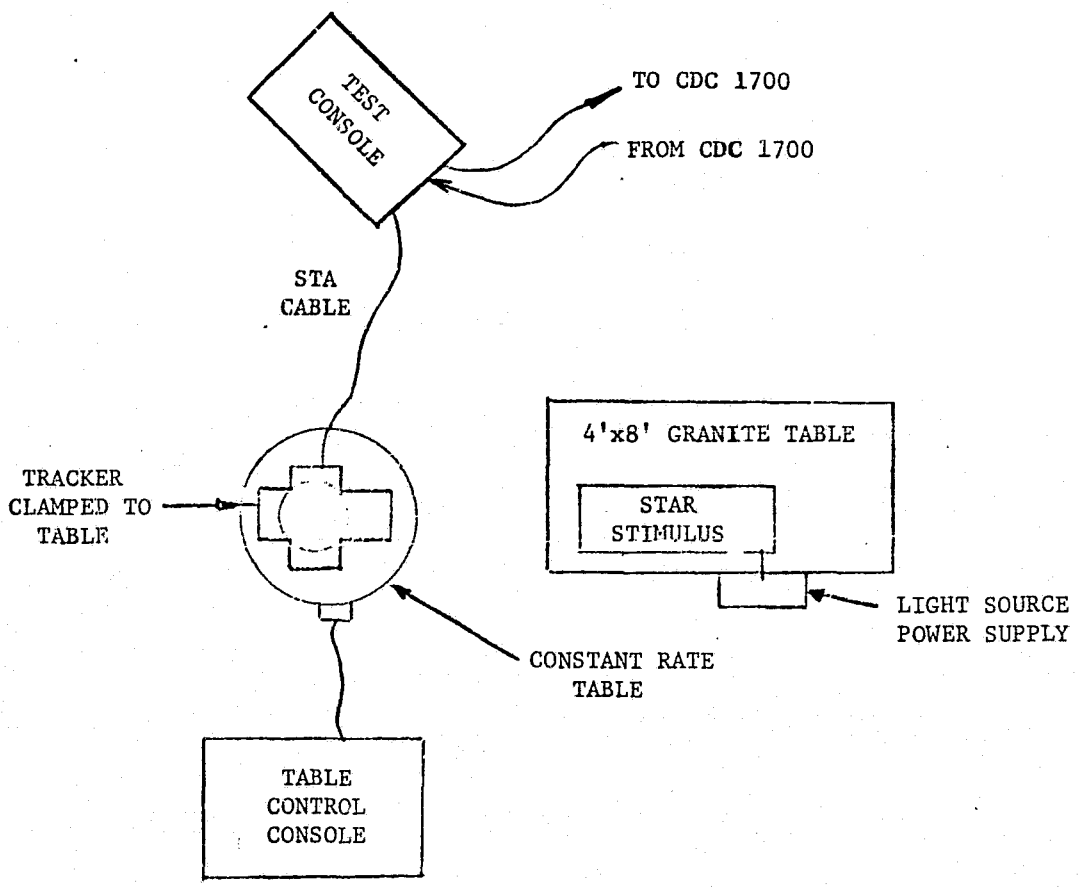

FIGURE 3. MOVING BASE TEST FACILITY

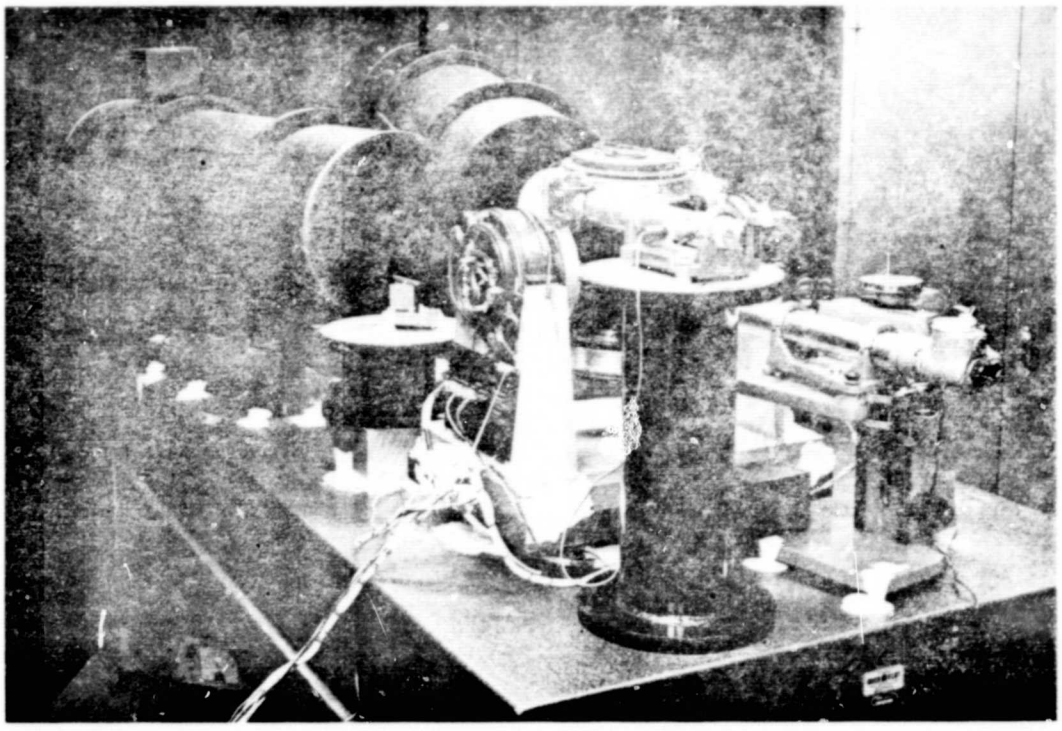

FIGURE 4. FIXED BASE TEST FACILITY

Large tubes in background are the 12 inch diameter (500 inch focal length) star sources. Left autocollimator monitors outer gimbal motion and right monitors inner gimbal. A third autocollimator monitors star motion.

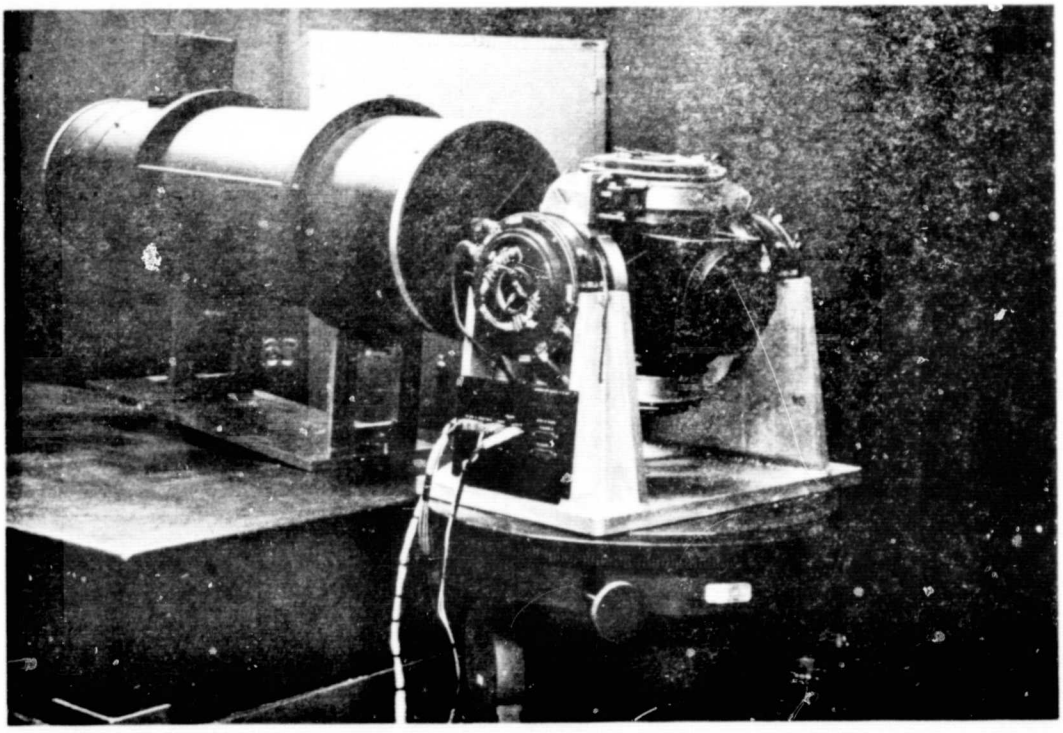

FIGURE 5. MOVING BASE TEST FACILITY

Table motion is in horizontal plane. Rates 0.01-05 deg/sec were investigated in the study.

the SSU. Autocollimation of these surfaces was used to measure the relative motion of the SSU with respect to the outer gimbal, to the star reference, and to the angle calculated from the 360-speed encoder electrical signals.

Moving Base

This facility layout, shown in Figure 3 consisted of one star stimulus and the STA mounted on an Inland Precision rate table. The purpose of this test was to demonstrate the ability of the tracker and the control systems to function under conditions similar to spacecraft motion.

Star Sources

The star sources were 12-inch Cassegrain telescopes with Coude focus. Focal length was 500 inches. Light sources were GE 1960 lamp with diffuser and 50×10^{-4} in. pin hole.

Test Console

The test console provided regulated power, a computer control panel, scope displays, and amplifiers for the star tracker outputs. Demodulators and filters for the Inductosyn processing were also mounted in the console. The test console was also used as a central patch panel to interface the various equipment. Figure 6 shows a block diagram identifying the major interfaces.

Star Tracker Motor Drive and Gimbal Angle Readout

Motor drive and Inductosyn processing was provided by test gear simulating the Sensor Electronics Assembly. Each gimbal drive consisted of a pair of two phase 24-pole synchronous motors driven by the Inductosyn commutation loop shown in Figure 7. The 360-speed Inductosyn encoders were excited by a 10 kHz carrier producing a sine and cosine ac modulated signal which was demodulated, filtered and fed to a CDC 1700 digital computer. A digital software inverse tangent routine computed gimbal angle (incremental) from the 360-speed data and merged this with the accumulated count of the number and polarity of one degree increments traversed. The angle data was then used as the relative gimbal positions which in turn were used to generate the 12-speed sine and cosine data necessary to commutate the drive motors. Driven in this manner the motors have a dc torquer characteristic in the sense that motor torque was linearly dependent on the input command V_0. The gimbal angle could be readout from the computer or alternately, from the amplified sine/cosine Inductosyn outputs.

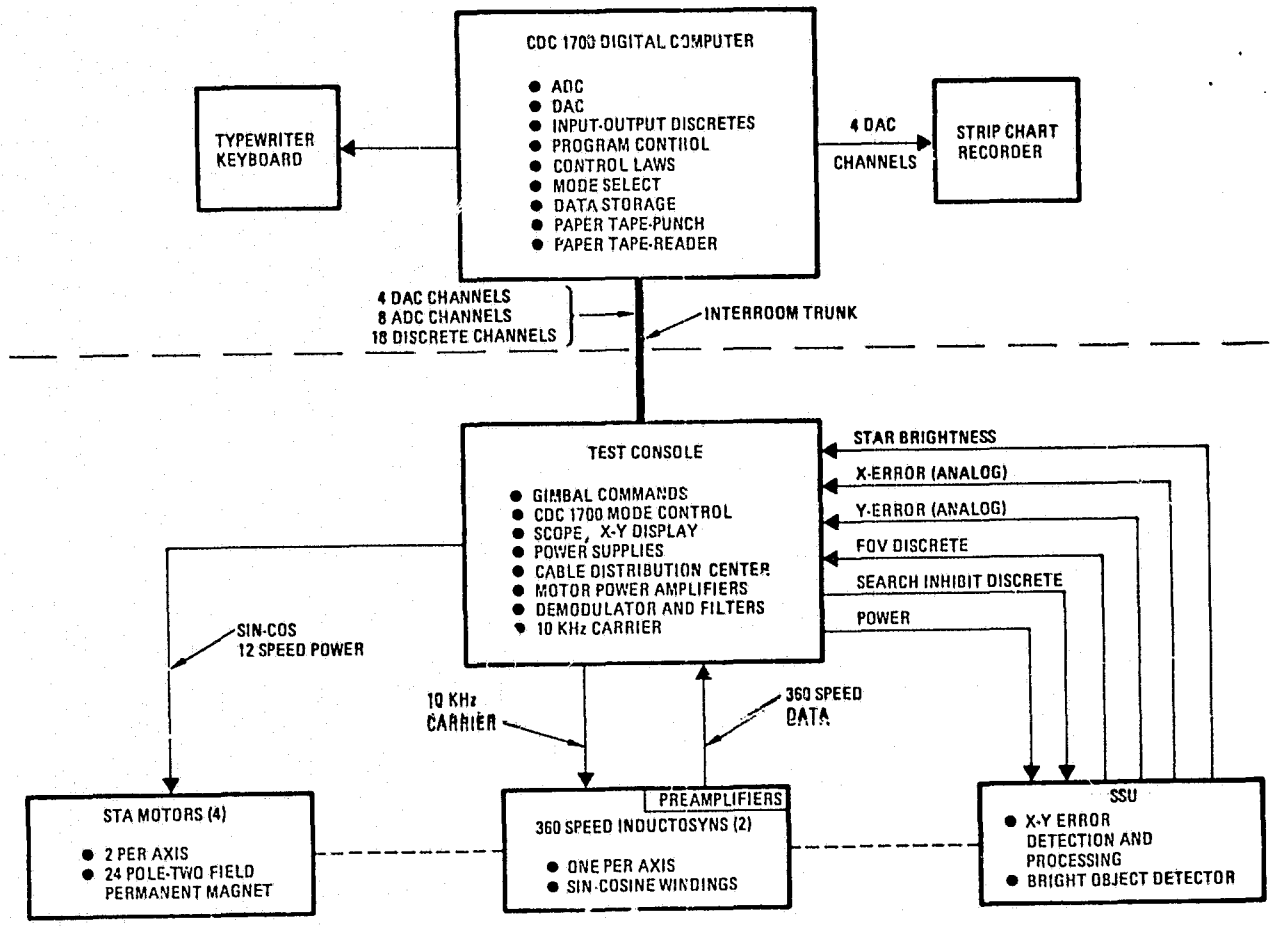

Figure 6. STA Lab Test Facility Equipment Functional Block Diagram

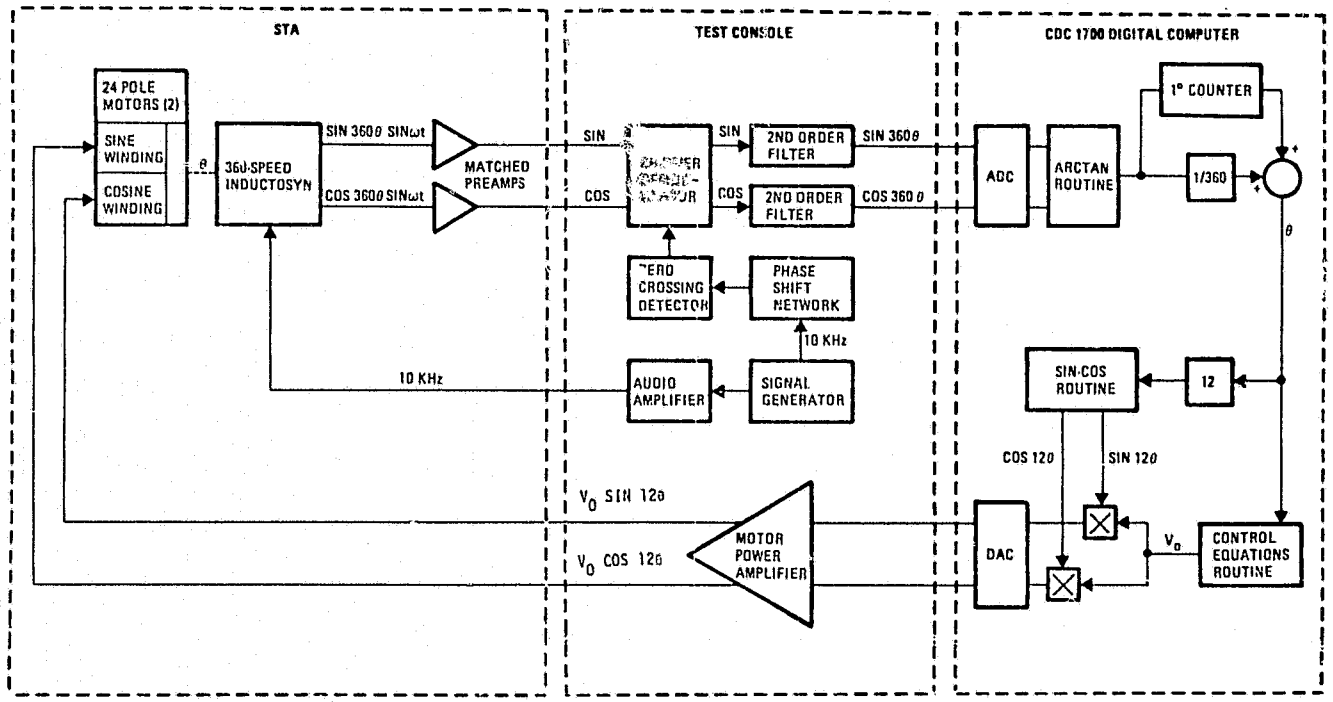

Figure 7. STA Lab Test Commutation Loop Functional Block Diagram

3.0 TEST RESULTS

3.1 Star Tracker Parameter Tests

A series of tests were run to measure significant design parameters of the star tracker (scale factors, friction, FOV, torques, etc.). During the motor torque and bearing friction tests, a design problem relating to the bearing suspension was discovered. The motor radial magnetic forces were larger than the designed radial restraining force induced by the bearing preload, which allowed the gimbal axes to be slightly displaced. The increased bearing preload used to counteract this problem led to the rather high friction readings shown in the test results. Other test results were thought not to be affected by this change.

Star Sensor Scale Factor

Scale factor measurements were made by moving (manually) the star sensor until the star sensor output reached a particular voltage (see Figure 8) and then reading the star sensor position relative to the star source with an autocollimator. Repetitive runs were made as shown in Figure 8. Average scale factor was 20mv/$\widehat{sec}$, confirming early star sensor unit test results.

Star Sensor FOV

The acquisition FOV of the star sensor was measured by moving (manually) the sensor toward the star source and noting where the "star acquired" discrete was set. Figure 9 shows the results. The design FOV is ± 5 $\widehat{min}$ in each axis. The test data indicated a larger total FOV in both axes with an asymmetry apparent in the horizontal axis. The cause of this discrepancy has not been determined. Earlier test on the star sensor did not show this problem.

The data showing where the discrete turned off were obtained by moving the sensor away from the star. No design value exists for how far tracking can occur. It is dependent on photocathode area and electronics saturation effects.

Star Sensor Noise

Output noise parameters were obtained from strip chart recordings of the analog signals. Chart speeds of 2, 5, 10 and 20 cm/sec were used. The mean square error of 100 equally spaced data points for each speed is given in Table 1.

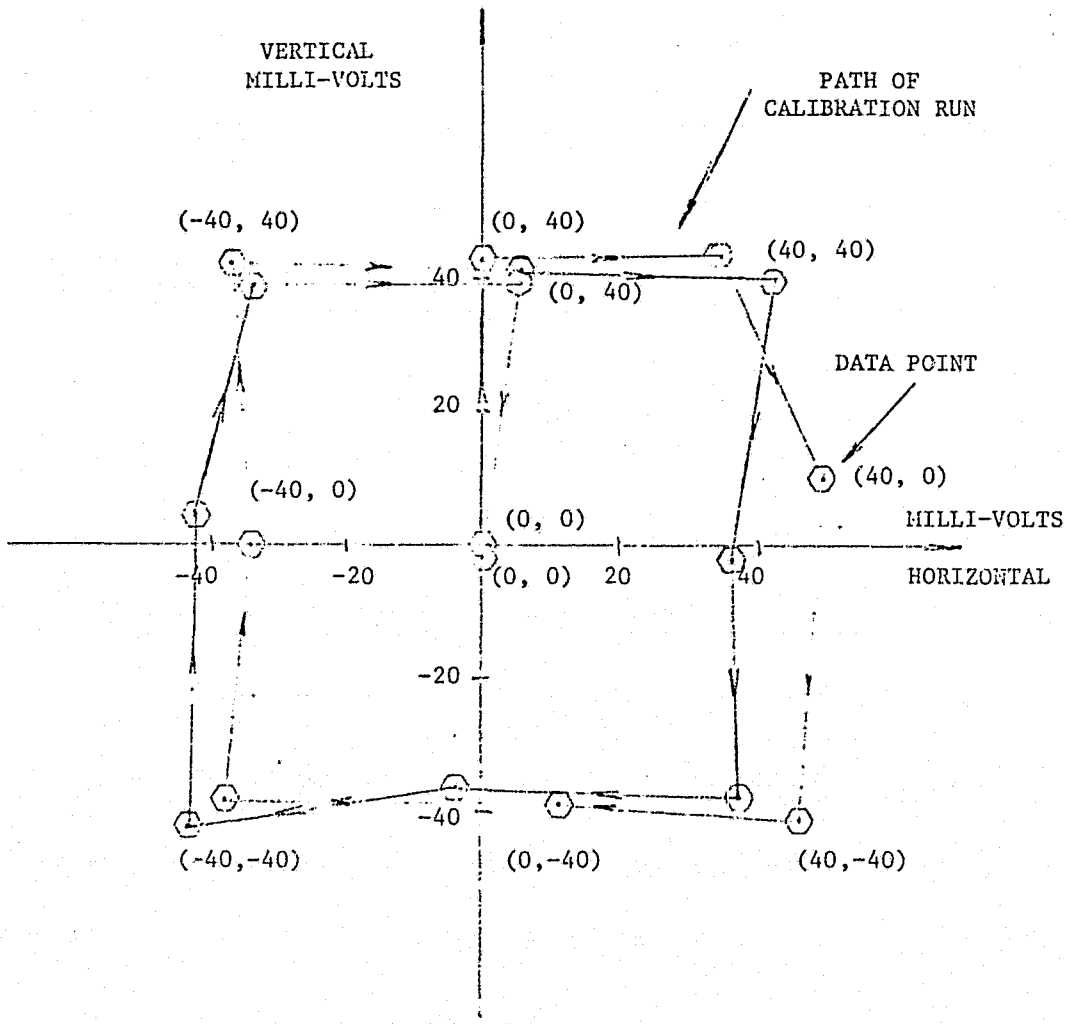

OPTICAL READINGS TAKEN AT THE SSU OUTPUT VOLTAGES SHOWN IN MILLIVOLTS.
DATA POINTS TAKEN ON A SQUARE ±2 ARC-SEC

FIGURE 8. STAR SENSOR SCALE FACTOR

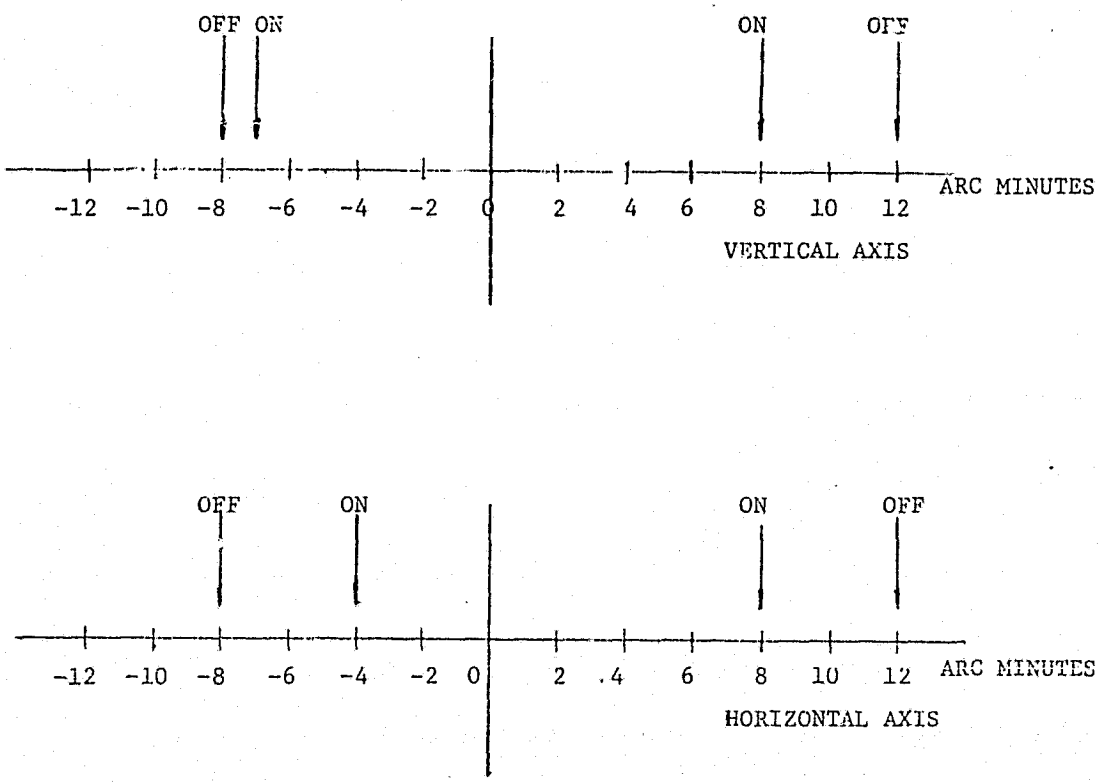

FIGURE 9. SSU FIELD OF VIEW

Table 1. Sensor Noise Figure Taken From Strip Chart Recordings. Star 3.5 Mv

Chart Speed	Standard Deviation arc-sec
2 cm/sec	1.01
5 cm/sec	1.11
10 cm/sec	0.815
20 cm/sec	0.77
RSS	0.935

These noise measurements were made on a +3.5 M star for which the predicted noise is 0.35 sec (1σ). Earlier star sensor measurements had confirmed this lower value. Other recordings of sensor output signals show significant facility generated noise when the sensor is turned off. This is thought to explain the difference in data.

Motor Power Amplifier Gain

Typical gain characteristics for the sine and cosine amplifiers appear in Figure 10. Each had a nominal slope of 3.5 v/v. The amplifier bandwidths measured at the 3 db down point were in the range 50-80 Hz. Gain was essentially flat to this range. No hysteresis or deadzones were detected in the voltage range of interest.

Motor-Gimbal Parameters

Gimbal inertia and friction was determined through ramp tests. In this test a constant torque, slightly larger than the motor breakaway torque, was applied through the motor to the gimbal shaft. The torque was held for a length of time and then removed allowing the rate to return to zero under the influence of the gimbal friction. Rate measurements were then obtained. The maximum rate was held at low levels to minimize the effect of viscous friction but high enough to avoid compliance effects. A typical run is shown in Figure 11. Assuming a simple model where

t_d = decay time
t_a = time motor torque applied
$t_a + t_d$ = time for rate to return to zero
τ_m = motor torque
τ_c = gimbal friction
$\Delta\dot{\theta}$ = rate change at t_a

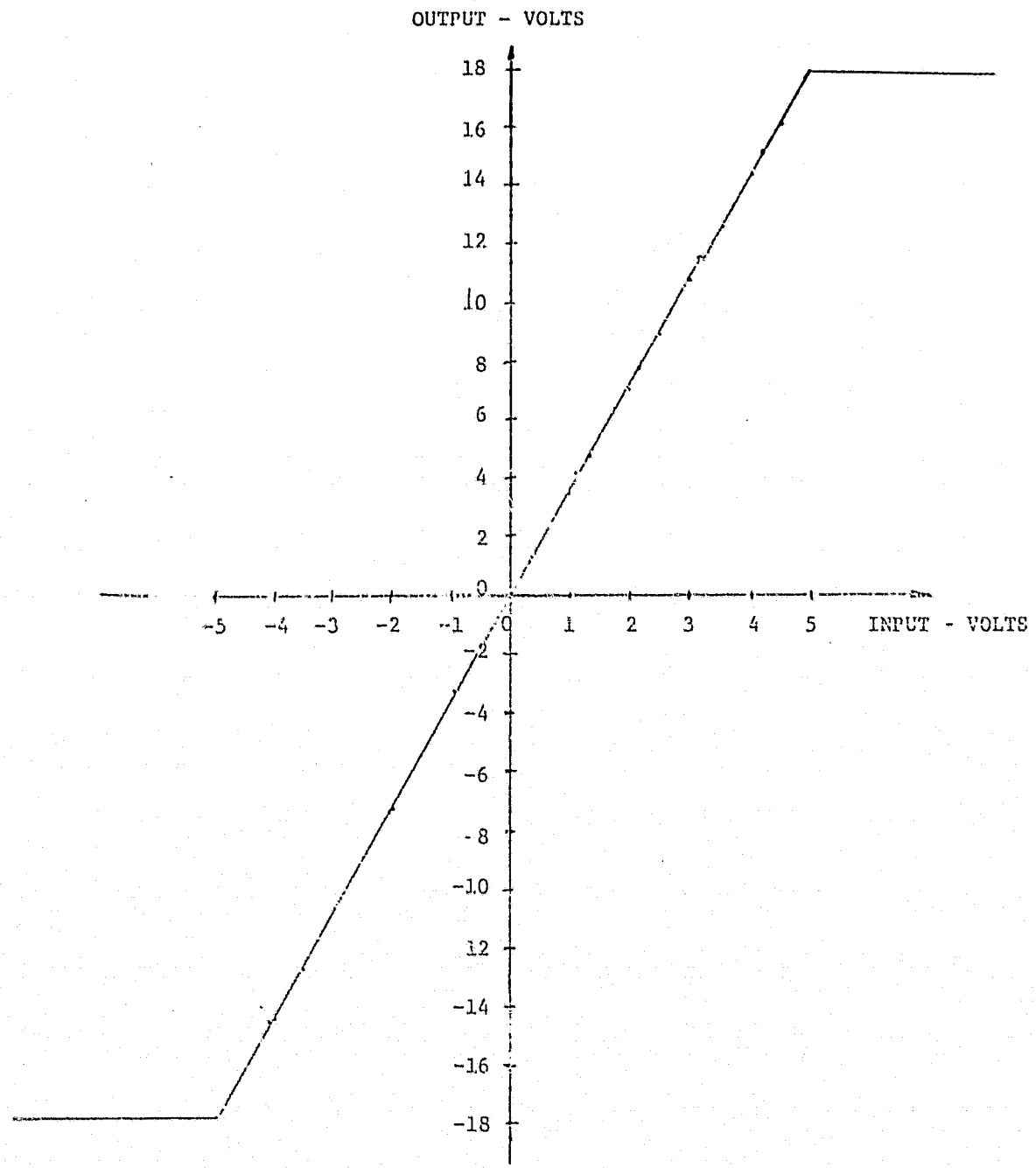

FIGURE 10. TYPICAL POWER AMPLIFIER GAIN CHARACTERISTIC

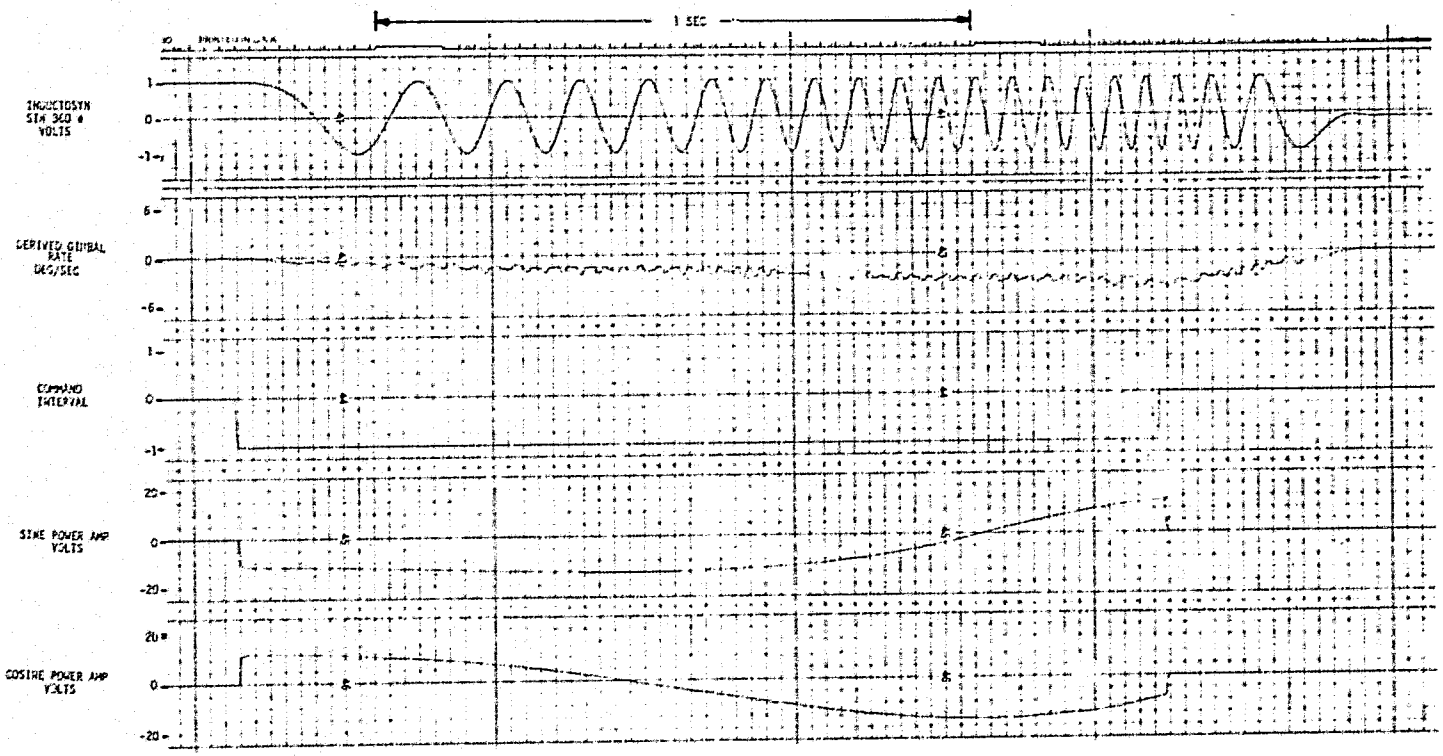

FIGURE 11. TYPICAL GIMBAL RAMP TEST

then the gimbal friction was computed as

$$\tau_c = \frac{\tau_m \, t_a}{t_a + t_d}$$

and the gimbal inertia as

$$I = \frac{\tau_m \, t_a \, t_d}{\Delta\dot{\theta}(t_a + t_d)}$$

The results of this test are summarized in Table 2.

Table 2. Summary of Ramp Test Results

Axis		Friction ft-lb	Inertia$_2$ slug-ft^2
Inner	+ Rate	0.385	0.124
	- Rate	0.317	0.121
	Average	0.351	0.123
Outer	+ Rate	0.532	0.490
	- Rate	0.570	0.520
	Average	0.551	0.505

Motor Torque Versus Voltage

Motor voltage-torque characteristics were found using a torque watch. A large scale factor device was used to hold the angular excursions to less than ± 2 deg. Under this condition voltages could be applied directly to the power amplifiers without the need of commutation if the sine and cosine winding voltages were gained according to the nominal commutation point. The results of the test are shown in Figure 12. Hysteresis effects shown in these figures imply coulomb friction and the values shown correlate well with those in Table 2 for the ramp test and also with analytically derived values based on the increased bearing preload used to correct the bearing suspension design problem.

Drive-Sensor Frequency Response

A frequency response of the transmittance between the motor voltage and SSU output for each axis was obtained. The results of this test appear in Figures 13 and 14. Several voltage input levels were used in the test as a means of

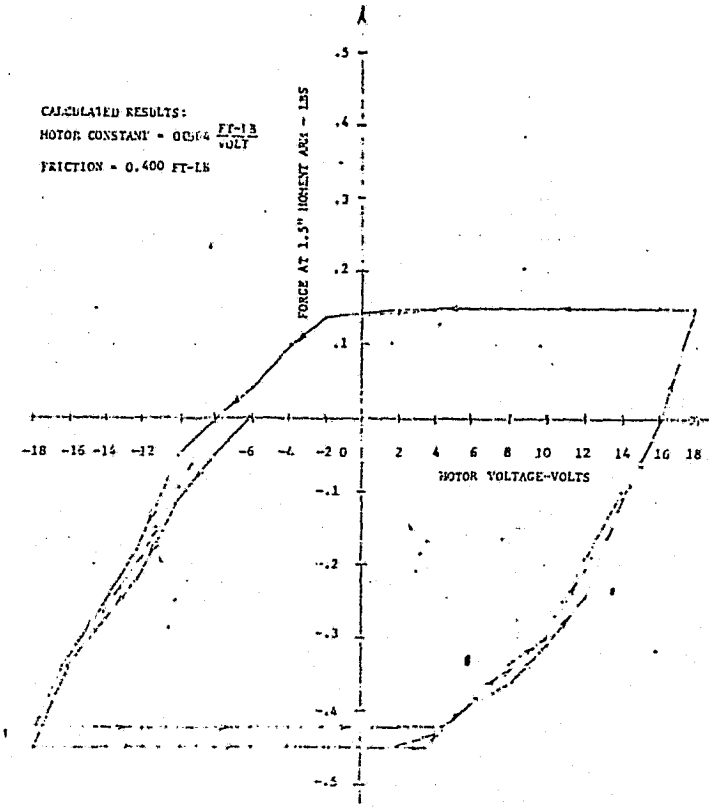

FIGURE 12a. OUTER GIMBAL TORQUE

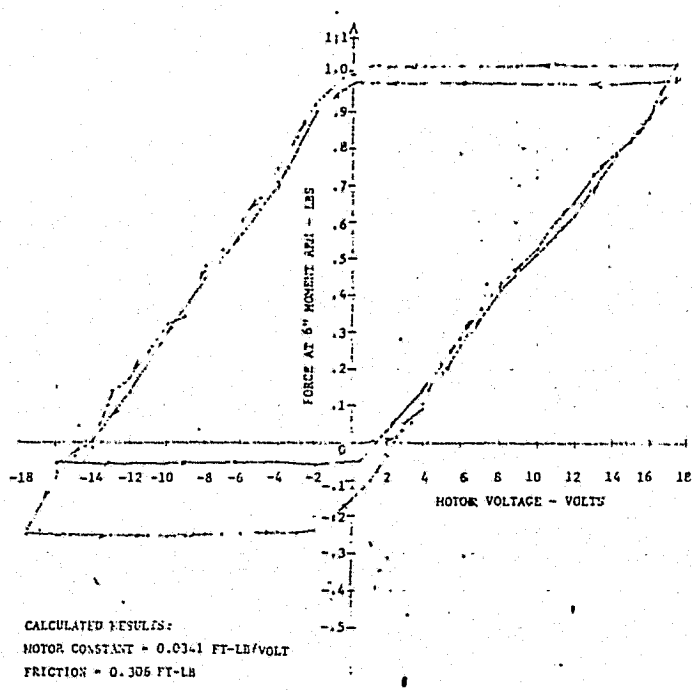

FIGURE 12b. INNER GIMBAL TORQUE

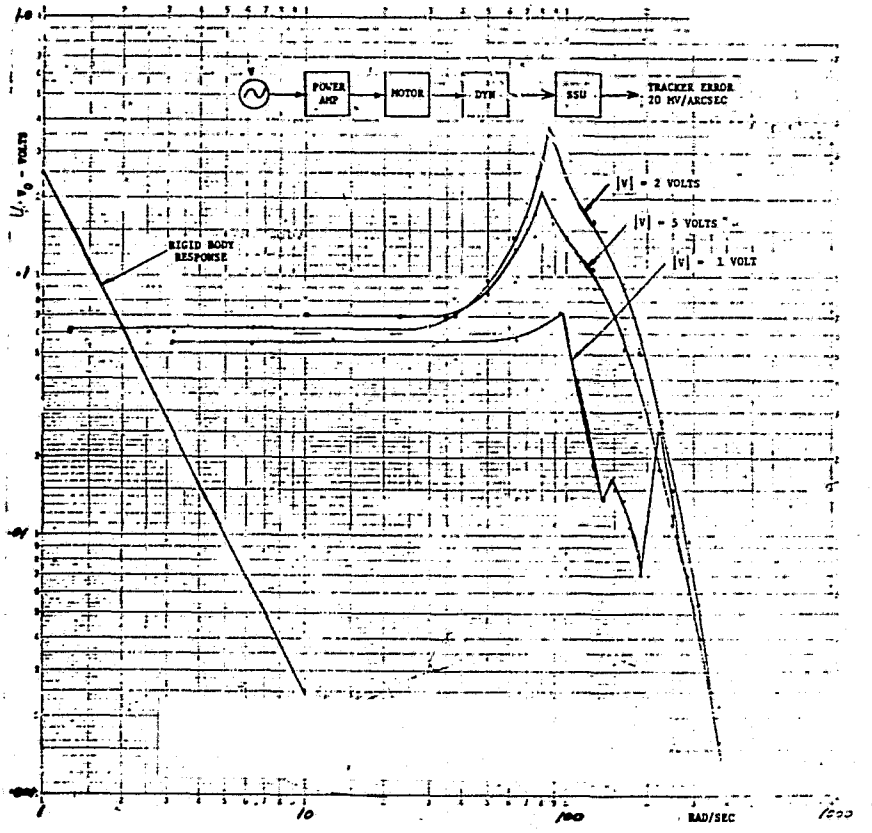

FIGURE 13. OUTER GIMBAL FREQUENCY RESPONSE

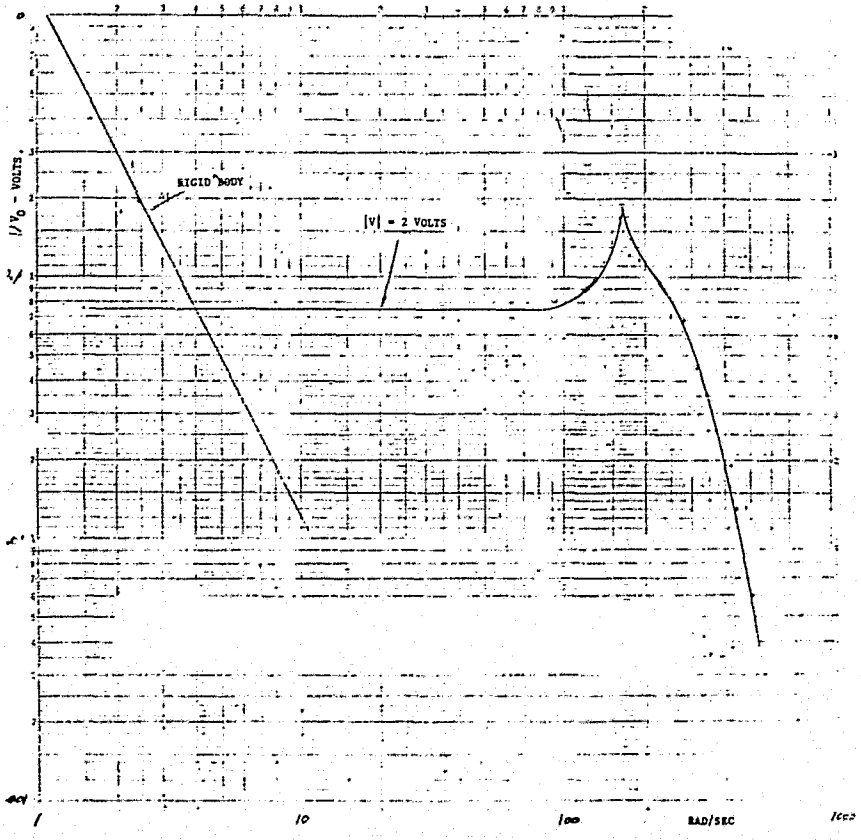

FIGURE 14. INNER GIMBAL FREQUENCY RESPONSE

determining the influence of friction on the tests. Observation of the frequency response data indicates that most motion in the +20 $\widehat{sec}$ range is due to the bending of a compliance circuit rather than the gimbal sliding on the ball. This hypothesis is supported by three features of the frequency response. The first is that SSU movement is detected for motor torques less than the breakaway value; secondly, the phase shift and amplitude at low frequencies at maximum motor torque indicate a constant gain function rather than the rigid body sharp roll off of 40 db/decade; and, finally the reasonance peak detected at 20 Hz.

Using the inertias in Table 2 and a simple spring mass model, the inner gimbal effective rotating stiffness is K_e = 2000 ft-lb/rad, and the outer gimbal stiffness is K_e = 3600 ft-lb/rad. These values are a factor of about 3 below the predicted stiffness. The most probable cause of this lower stiffness has been determined to be due to static bending of the bearing suspension flexure caused by the larger preloads which were used (noted earlier). Analysis of the bearing suspension stiffness under the bending measured (0.016" deflection) shows a factor of 3 reduction below the design value.

3.2 Functional Tests

A series of tests were run to demonstrate star tracker functional characteristics (slew, lock-on, track).

Slew and Lock-On Test

The first closed loop dynamic test was a check of slew and transient performance. The test consisted of cycling the tracker between two +3.5 magnitude stars. Both the tracker base and the star were inertially fixed.

The star acquisition sequence was fully automated as a subroutine in the digital program. The transient performance in terms of gimbal angles and star tracker error signals was displayed on strip chart recorders or stored as bulk data in the digital computer. A typical large angle run is shown in Figure 15.

Performance of the gimbal was very close to that predicted by analog simulation. The effect of zercing all integrators before executing the SSU control worked well and, as predicted, allowed a smooth transition from gimbal control by causing the system to be stopped momentarily in the gimbal friction while the SSU integrator was building up a torque sufficient to exceed the friction.

The slew and lock-on was executed well. No misses attributed to the control were noted. In all cases (the star simulators were moved several times), the Inductosyn control was able to bring the SSU FOV within 1 $\widehat{min}$ of the star.

FIGURE 15. SLEW AND LOCK-ON PERFORMANCE

Tracking Test

Tracking tests were conducted by driving a precision rate table at a fixed rate with the SSU locked onto the star image. The table rate was reversed after a specific table angle had been traversed. The table acceleration was controlled through the rate table drive electronics to be less than 0.01 deg/sec^2. Rates investigated were in the range 0.01 to 0.50 deg/sec.

Figure 16 shows tracking performance with 0.3 deg/sec table rate. Steady state tracking error was 1.3 $\widehat{\text{sec}}$. Maximum error during turn around was $\pm$20 $\widehat{\text{sec}}$.

3.3 Repeatibility and Stability Tests

Repeatibility

Repeatibility tests dealt with the ability of the STA to return mechanically and optically to the same location. This directly checked Inductosyn accuracy, control system accuracy, material hysteresis, bending effects, bearing errors, and thermal effects.

The repeatibility test consisted of the sequence:

- Command tracker to star
- Allow automatic SSU lock-on
- Hold for 80-100 seconds
- Command tracker off star (several degrees both axes)
- Repeat sequence

This sequence was performed many times in order to accumulate sufficient data to arrive at a statistical measure of repeatibility. A few cycles of this test are shown in Figure 17. Information taken from the STA Inductosyns electrical signals, optical measurement of outer gimbal vertical motion and SSU vertical and horizontal motion measurements were relative to initial readings. The test was run after the star and STA thermal systems had reached a relative steady-state (normally a 60-90 minute waiting period).

Both axes proved to have similar performance. The errors measured are shown in Table 3. Optical autocollimator measurements were made from the outer gimbal and the SSU mirror surfaces. The optical measurements in Table 3 are averages of five closely spaced readings. Electrical measurements were obtained from the SSU analog outputs and the reduction of the 360-speed Inductosyn data. Electrical signals were recorded at the test site rather than from the 1700 to increase the signal-to-noise ratio.

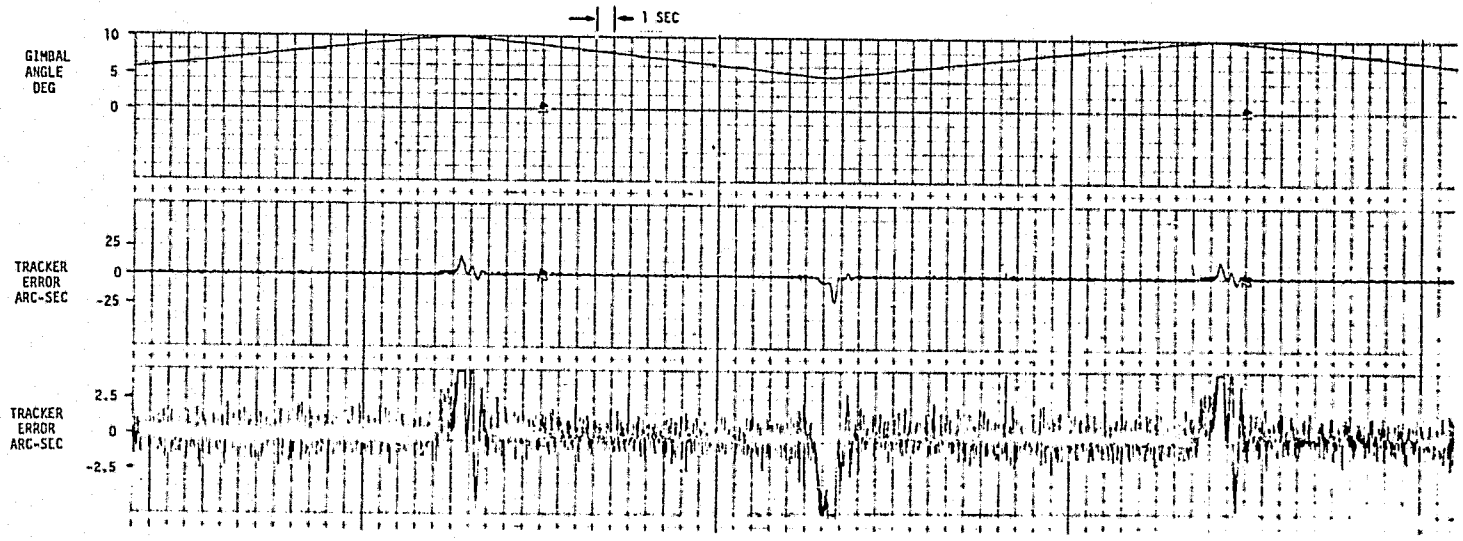

FIGURE 16. MOVING BASE TEST

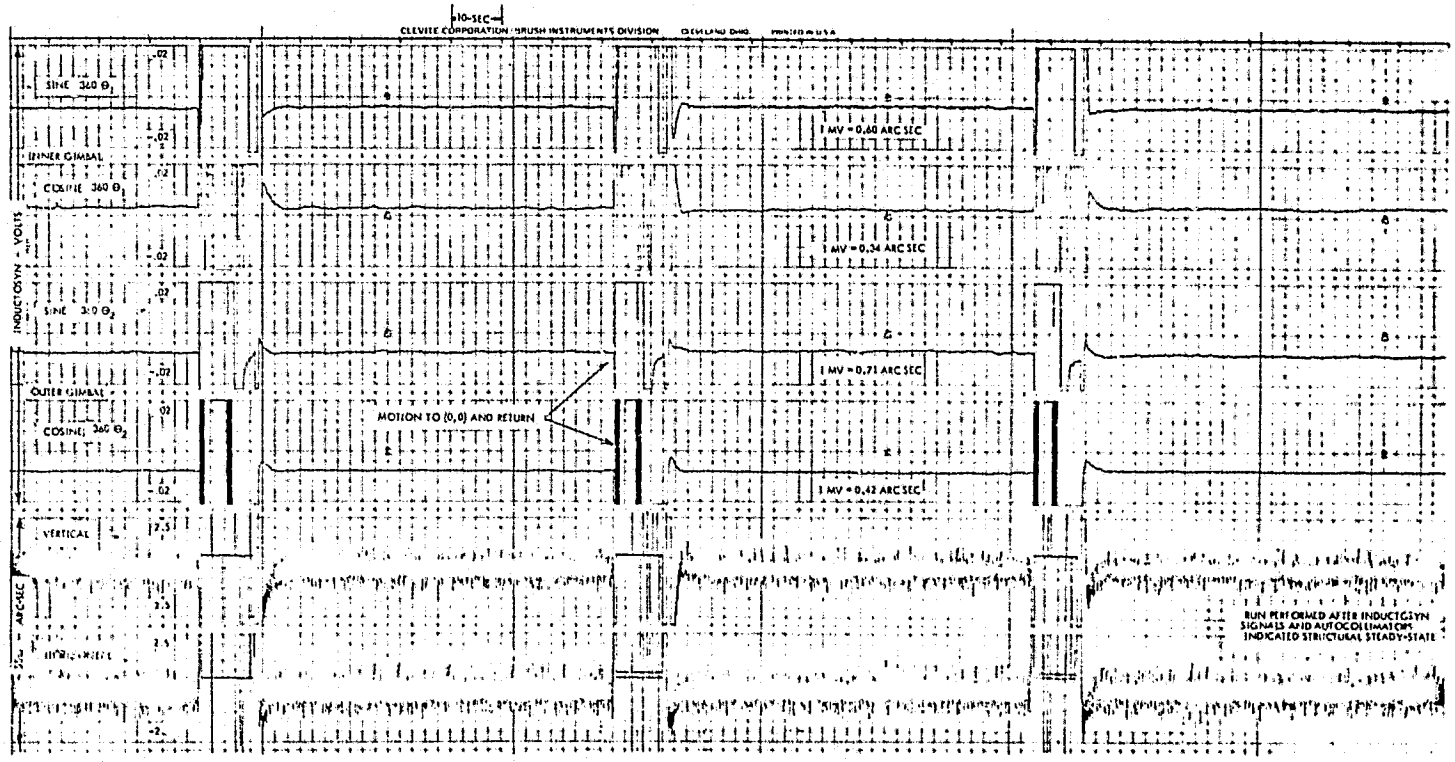

FIGURE 17. REPEATIBILITY TESTS

Table 3. Repeatability Test Results

Measurement Location	Repeatibility (arc sec)
SSU Mirror Surface(Optical)	0.5
Outer Gimbal (Optical)	0.3
Inductosyn (Electrical)	0.4
SSU (Electrical) (Noise)	0.935 (1σ)

The optical readings were obtained from an autocollimator having a resolution of 0.1 $\widehat{\text{sec}}$. Measurement accuracy obtainable by a given operator is probably a few tenths of an arc sec, so that sub-arc sec performance is difficult to verify. However, the results in Table 3 indicate repeatibility below an arc second.

Long Term Pointing and Tracking

This test was performed to obtain a measure of static offsets due to electrical, optical or mechanical biases over a period of several hours. Star visual magnitudes (Mv) of 1, +3.5, and +4.5 Mv were used in the test.

Optical readings were taken of the outer gimbal vertical motion, SSU vertical and horizontal motion, and the star vertical and horizontal motion during a test period of 60 minutes. Inductosyn signals were recorded at the test site. Table 4 shows the test results.

Table 4. Long Term Stability Test

Star Magnitude	Stability Measurement (arc sec)		
	Star Motion (Optical Reading)	Gimbal Motion (Optical Reading)	Induction (Electrical Reading)
+1	0.4	0.2	0.2
+3.5	0.7	0.3	0.3
+4.5	1.1	1.1	1.0

It was difficult to determine whether the apparent motion of the gimbal and Inductosyn were correlated with the star motion, due to the time required to make the optical readings (each optical reading is an average of 5 points). The data presented is an envelope of all readings taken during the stability test.

Star motions of 10 $\widehat{sec}$ or more were observed when changing star magnitude, indicating a heating problem in the star source. This motion did not affect the test results, which measured stability under steady state conditions.

4.0 CONCLUSIONS

- Functional performance of star tracker during slew, lock-on, and track modes was as expected.
- Star tracker repeatibility to less than 0.5 $\widehat{sec}$ was demonstrated.
- Star sensor noise of less than 1 $\widehat{sec}$ was demonstrated.
- Design problems associated with the bearing suspension have been identified and are easily corrected.
- The following suggestions are made to improve future testing when sub-arc-second readings are required:
  1) Better control of air conditioning
  2) Thermal control of star sources
  3) Use automated measuring equipment to allow remote operation and realtime data correlation.

5.0 REFERENCES

1. Final Technical Report, PPCS Functional Design, Analysis, and Error Analysis, D. K. Kirby, TRW Report No. 13900-6012-RO-00, July 1971.
2. An Integrated System for Precision Attitude Determination and Control, A. M. Frew, D. K. Kirby, P. C. Wheeler, and T. C. Huber, AIAA 1971 Guidance, Control, and Flight Mechanics Conference, August 16, 1971.
3. Ultra High Accuracy Gimbaled Star Tracker, R. F. Gates, D. Eisenhut, G. Zaremba, and J. Kalley, AIAA Guidance Control, and Flight Mechanics Conference, August 16, 1971.
4. PPCS Note 75, Preliminary Modal Analysis of PPCS STA Gimbal Assembly, F. S. Snively.
5. PPCS Note 136, Design and Analysis of PPCS STA Gimbal Servo Track Mode, F. S. Snively.